DISCLAIMER

This report was prepared as an account of work sponsored by an agency of the United States Government. Neither the United States Government nor any agency thereof, nor any of their employees, makes any warranty, express or implied, or assumes any legal liability or responsibility for the accuracy, completeness, or usefulness of any information, apparatus, product, or process disclosed, or represents that its use would not infringe privately owned rights. Reference herein to any specific commercial product, process, or service by trade name, trademark, manufacturer, or otherwise does not necessarily constitute or imply its endorsement, recommendation, or favoring by the United States Government or any agency thereof. The views and opinions of authors expressed herein do not necessarily state or reflect those of the United States Government or any agency thereof. Reference herein to any social initiative (including but not limited to Diversity, Equity, and Inclusion (DEI); Community Benefits Plans (CBP); Justice 40; etc.) is made by the Author independent of any current requirement by the United States Government and does not constitute or imply endorsement, recommendation, or support by the United States Government or any agency thereof.

ORNL/TM-2025/3964

CRADA Report NFE2209377-BINDER JET ADDITIVE MANUFACTURING OF SILICON CARBIDE SOLAR REACTOR

Trevor Aguirre
Amy Elliott
Corson Cramer
Kashif Nawaz

June 2025

OAK RIDGE National Laboratory

ORNL IS MANAGED BY UT-BATTELLE LLC FOR THE US DEPARTMENT OF ENERGY

FINAL REPORT CERTIFICATION (ORNL-851)

Final Report Certification
for
CRADA Number NFE2209377

Between

UT-Battelle, LLC

and

Dimensional Energy, Inc.
(Participant)

Instructions:

Mark the appropriate statement in 1a or 1b below with an 'IX." Refer to the articles in the CRADA terms and conditions governing the identification and marking of Protected CRADA Information (PCI).

If no PCI is identified, the report will be distributed without restriction. If PCI is identified, the report distribution will be limited in accordance with the CRADA terms and conditions governing release of data. In all cases items 2 and 3 must be true. That is, the report cannot contain Proprietary Information and a disclosure must be filed prior to release of the report.

The following certification is made for the subject final report:

1. (a) ☐ The final report contains information that qualifies as "Protected CRADA Information" (PCI). The PCI legend is printed on the report cover, and the PCI is clearly identified.

OR

(b) ☒ The final report does not contain "Protected CRADA Information." The "Approved for Public Release" legend is printed on the report cover.

2. The final report does not contain Proprietary Information.

3. By the signature below, the Participant has no objection to the public distribution of the final report due to patentable information.

For the Participant:

Bradley J. Brennan, CSO
(Name and Title)

Bradley J. Brennan
(Signature)

6/26/2025
(Date)

ORNL/TM-2025/3964

Manufacturing Science Division

CRADA REPORT NFE2209377- BINDER JET ADDITIVE MANUFACTURING OF SILICON CARBIDE SOLAR REACTOR

Trevor Aguirre
Amy Elliott
Corson Cramer
Kashif Nawaz

June 2025

Prepared by
OAK RIDGE NATIONAL LABORATORY
Oak Ridge, TN 37831
managed by
UT-BATTELLE LLC
for the
US DEPARTMENT OF ENERGY
under contract DE-AC05-00OR22725

CONTENTS

LIST OF FIGURES

LIST OF TABLES

ABBREVIATIONS

ORNL	Oak Ridge National Laboratory
BJAM	Binder jet additive manufacturing
CVI	Chemical vapor infiltration
SiC	Silicon carbide
PSD	Particle size distribution
ASTM	American Society for Testing and Materials
PDF	Probability Density Function
CDF	Cumulative Distribution Function

ABSTRACT

Achieving high powder packing density is critical in binder jet additive manufacturing (BJAM), as it directly influences the final part density, mechanical properties, and sintering behavior. Multi-modal powder blends, which combine particles of different sizes, have been explored as a strategy to optimize packing efficiency and minimize defects. In this study, bimodal and trimodal powder blends were obtained by mixing silicon carbide powder in three different sizes. These results show that increased powder density is achievable with bimodal powder blends but is reduced in trimodal blends, and it was found that a 13% increase in the powder tap density was achieved using a bimodal blend of powder. The powder size distribution of the bimodal blend was measured at various stages during binder jet additive manufacturing and, no measurable powder separation occurred even after eight prints. Overall, this study shows limited advantage to trimodal powder blends but good promise for trimodal blends for increasing printed density while maintaining reusability in the binder jet process.

1. INTRODUCTION

Binder jetting additive manufacturing (BJAM) is a valuable technology for shaping non-weldable materials—such as silicon carbide (SiC)—into complex geometries used in advanced applications like solar reactors for power generation. The BJAM process involves spreading a thin layer of powder across a print area and selectively depositing a binder using an inkjet printhead in the shape of each part layer. These steps are repeated layer by layer until the full part is formed. After printing, the part is typically cured or dried and removed from the powder bed for post-processing. Because the printed part is only loosely held together at this stage, it requires further processing—such as sintering or infiltration—to achieve final mechanical integrity.

For SiC components used in solar reactors, chemical vapor infiltration (CVI) is often used as a post-processing method to densify the part and produce the desired alpha-phase SiC within the void spaces. One of the most effective ways to reduce CVI time and improve final part properties is to maximize the printed green density of the powder preform. Higher initial powder density reduces void volume, leading to improved strength and dimensional stability in the final component.

This study investigates the use of multi-modal powder blends to enhance powder packing in BJAM. While previous research has explored packing improvements through methods like in-situ compaction [1], powder blending—specifically bimodal and trimodal particle size distributions—offers a practical, print-process-compatible way to increase green density. Building on past studies and a known peak in packing efficiency at specific particle size ratios, the present work evaluates the potential of such blends in SiC powders, which differ significantly from idealized spherical particles in both shape and surface morphology.

The goals of this study were to:

1. Identify the optimum ratio of SiC particle sizes in bimodal and trimodal blends to maximize packing density.
2. Investigate the reusability and segregation behavior of such blends within a BJAM system.

This was accomplished by studying, powder blends that were systematically prepared by incrementally adding secondary and tertiary particle size fractions and measuring the resulting apparent and tapped densities. Once the optimal blend was identified, it was tested for recyclability by running it through a BJAM printer and sampling powder from various locations in the system to evaluate changes in particle size distribution and segregation behavior.

2. BACKGROUND

2.1 LITERATURE REVIEW

Prior work sought to improve powder packing in BJAM through both experimental and computational methods [1–8]. These studies have shown that packing behavior is stochastic and influenced by factors such as particle size, shape, distribution, density, and surface morphology, with typical theoretical packing densities ranging from 50–60%. One commonly explored strategy involves adding fine powders to fill the void spaces between larger particles. For bimodal blends, optimal density improvements have been observed when the size ratio of large to small particles is approximately 7–10:1 [9].

Additional research has expanded on bimodal systems [2,10–14] and investigated trimodal blends [9] as a means of further increasing density. However, many of these models assume smooth, spherical particles—a valid assumption for spheroidized powders [15,16], but not for irregular, faceted materials like SiC. Moreover, advanced packing models often rely on material parameters (e.g., surface energy, cohesivity, specific surface area) that are not readily available for many ceramic systems.

Notably, one prior study combining modeling and experimentation demonstrated a 5% increase in green density using bimodal SiC blends [17]. Building on these findings, the current work aims to further explore the potential of trimodal particle blending to improve powder packing and assess its viability in a realistic BJAM workflow, including powder reuse.

While prior studies have laid important groundwork in understanding particle packing behavior, there remains a need for systematic, experimentally grounded studies that reflect the realities of BJAM using irregular ceramic powders like SiC. The current work addresses this gap by quantitatively evaluating the impact of bimodal and trimodal blending on powder packing density, and by assessing the stability and segregation of these blends during actual use in a binder jet printing system. The following section outlines the experimental approach used to prepare, characterize, and evaluate these powder blends.

2.2 MATERIALS AND METHODS

2.2.1 SiC Powder

Two types of silicon carbide (SiC) powders were used in this study. A 23 µm SiC powder from Sigma-Aldrich was used as the unimodal reference, as it is commonly printed at Oak Ridge National Laboratory (ORNL) due to its relatively high flowability and packing density [18–24]. Additional SiC powders with average particle sizes of 37 µm, 12 µm, 4 µm, and 0.6 µm were sourced from Washington Mills. Each of the powders were imaged using optical microscopy and shown in Figure 1. A TEM mesh was placed on a slide with transparent, double-sided tape, and powder was poured over the slide and tapped remove un-adhered powder. The resulting samples were imaged with backlighting on a standard optical microscope. The TEM grid used was mesh size 100 which corresponds to an opening of 230 microns, which is used as the scale for measurement. Along with the irregularity of each powder, the size differences between the powders can be clearly seen. Specifically, the finest powder (0.6 µm in Figure 1A) is almost indistinguishable with prominent agglomeration, and the coarsest powder (37 µm in Figure 1E) can clearly be seen to be very coarse in comparison.

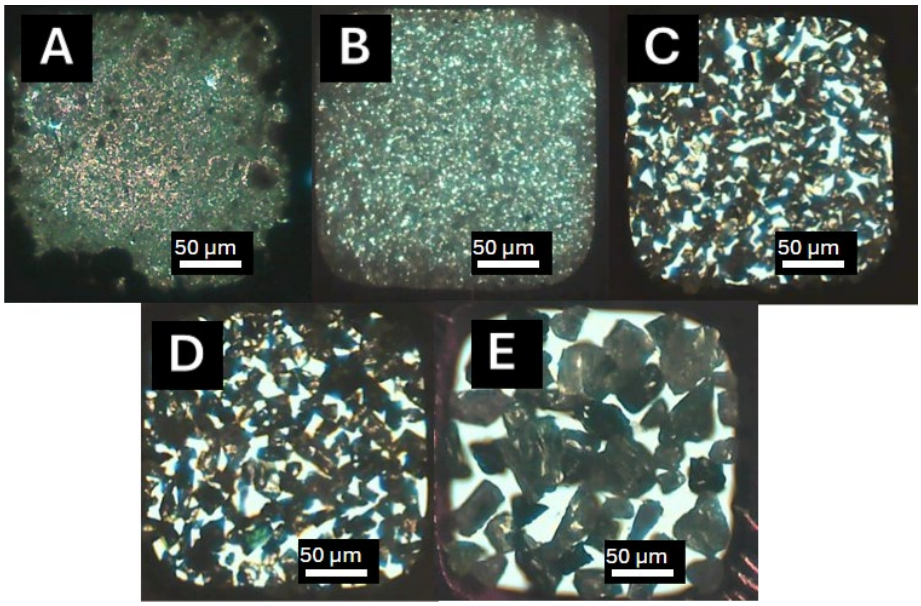

Figure 1: Powders utilized in the study imaged on a backlit microscope within a TEM grid for scale. They are A) Washington Mills 0.6 µm, B) Washington Mills 4 µm, C) Washington Mills 12 µm D) Sigma Aldrich 23 µm, E) Washington Mills 37 µm

2.2.2 Powder Sizing

The particle size distributions (PSD) of the SiC powders were measured using a MicroTrac laser diffraction system. Each powder sample was dispersed in deionized water and sonicated to break up agglomerations. The measurement was conducted at a flow rate between 25-30% flow, agitating the water and ensuring uniform suspension. The instrument reported a particle size based on a volume distribution. The PSD for the starting powders is shown in Figure 2. The powders distribution width increases with particle size. The 0.6 µm and 4 µm powders exhibit a narrow distribution around the average particle size, while the 23 and 37 µm powders exhibits a broader distribution.

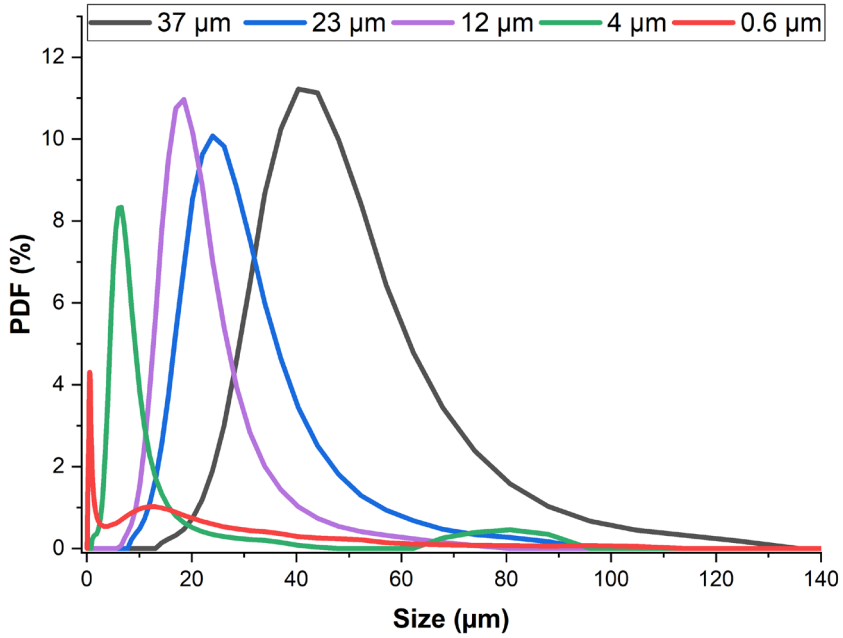

Figure 2: Starting powders PSD

2.2.3 Apparent and Tapped Density Measurement

Apparent density of the powder was measured in accordance with ASTM B212 [25] using a Hall flowmeter funnel and shown in Figure 3. The mass of powder required to fill a calibrated volume cup was recorded, and apparent density was calculated as the ratio of mass to volume. The tapped density of the powder blends was measured in accordance with ASTM B527 [26], which determines the density of metal powders by mechanically tapping a graduated cylinder until volume stabilization is achieved. The results below are the apparent and tapped density of the raw powders:

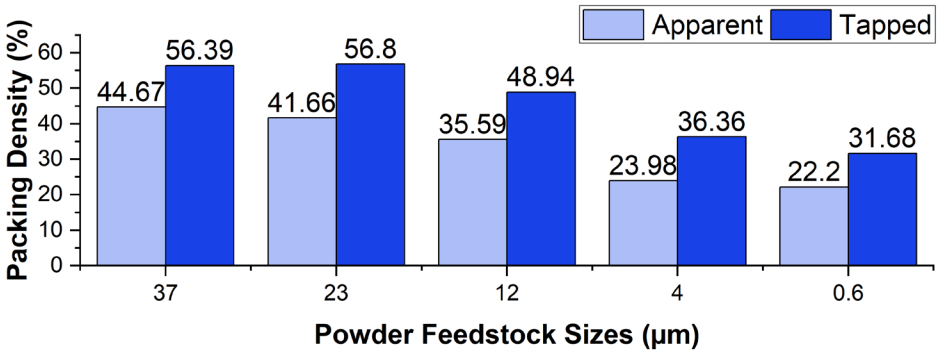

Figure 3: Apparent and tapped packing densities for individual SiC powders with varying particle sizes. Larger particles show higher packing efficiency, while smaller particles exhibit reduced flowability and increased interparticle voids.

2.2.4 Multi-Modal Powder Blending Procedure

To estimate the empty space between particles in the tapped powder, the solid volume was first calculated using the powder mass and the known material density. The tapped density was then used to determine the total volume the powder occupied. The difference between the total and solid volumes provided the volume of interparticle voids. Starting with the base powder, the medium sized powder was incrementally mixed into the base powder by pouring the blended powder through a riffle-type powder splitter (Humboldt Manufacturing Company, Figure 4 A-B) five times.

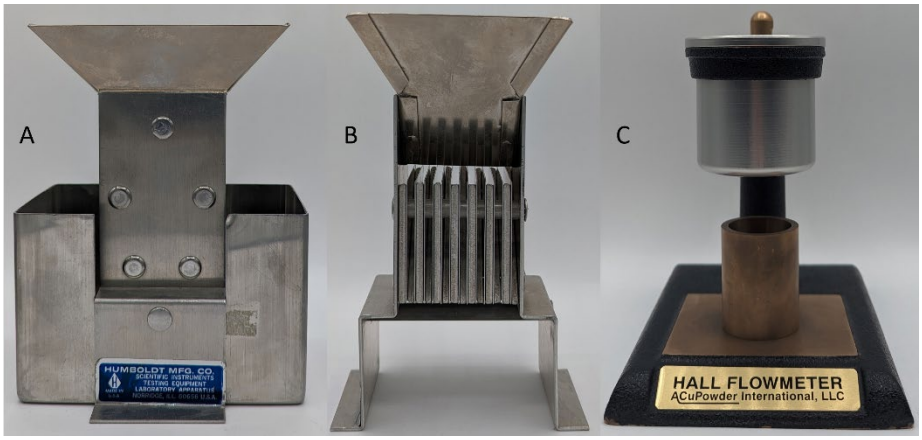

Figure 4: Powder splitter A) front view and B) side view and B) Hall-Flow Meter

To optimize powder packing density, a systematic blending approach was employed using a larger powder—either 37 µm or 23 µm SiC—as the starting material. The rationale for beginning with a larger/coarse powder lies in its relatively high flowability and the formation of large interparticle voids, which can then be efficiently filled with finer powders to increase packing density.

The void volume in the tapped base powder was first estimated using the known solid density of SiC and the measured tap density. Based on this, a calculated volume of finer powder was incrementally added to fill the void space. The first addition consisted of an amount of secondary (medium-sized) powder equivalent to 50% of the estimated interparticle void volume of the larger particle. This conservative starting point ensured partial filling without over-saturation, allowing better flow retention and preventing overpacking that could reduce powder mobility.
Subsequent additions of finer powder were made in increments of 0.05 times the original void volume, and the apparent and tapped densities of each blend were measured. This process continued until diminishing returns were observed in packing density improvements. In select trials, a third (finer) powder was introduced following the same approach—added in relation to the remaining estimated void space—to explore the benefits of trimodal blending.
This tiered blending strategy—starting with a coarse base powder and sequentially incorporating smaller particles—was designed to emulate theoretical models of multi-modal packing, where smaller particles fill the interstitial voids left by larger ones, ultimately minimizing total pore volume and maximizing solid loading.

2.2.5 Multi-Modal Powder Blending Procedure

To evaluate changes in particle size distribution (PSD) during repeated use of multimodal SiC blends in binder jetting, powder samples were collected throughout the printing process on an ExOne Innovent printer (Figure 5). For each of eight consecutive print runs, samples were collected from four locations: the hopper before printing, and the hopper, job box, and overflow reservoir after printing. This allowed assessment of potential powder segregation or attrition across the powder handling system.
Samples were extracted from the center of each region using a scoopula to minimize bias from edge effects or localized compaction. Care was taken to avoid contamination or layering artifacts during collection. All samples were stored in clean, labeled containers prior to analysis.

Figure 5: Innovent Printer from ExOne

The PSD of the starting powders and all collected samples was measured using a MicroTrac laser diffraction system. Measurements were performed in triplicate, and powders were dispersed in deionized water with sonication to reduce agglomeration. A small amount of surfactant was added as needed to promote uniform dispersion. The reported PSD values include D10, D50, and D90 metrics, which correspond to the particle diameters at 10%, 50%, and 90% of the cumulative volume distribution, respectively. This analysis enabled comparison of any shifts in PSD due to powder reuse, mechanical handling, or preferential transport of finer or coarser particles within the BJAM process.

2.2.6 Flexural Strength

The strength of print parts was measured in 4-point bending per ASTM C1161 [27] using Type B bars. The mean flexural strength was analyzed using a One Sample T-Test to determine if strength was different between the groups of printed specimens was different. The mean of samples printed with a bimodal powder distribution were tested to determine if the mean was significantly different from samples printed with a unimodal powder distribution.

3. RESULTS

3.1 BLENDED POWDER VOLUME FRACTIONS AND PACKING DENSITIES

As previously mentioned, to evaluate the effectiveness of multimodal powder blending in improving powder packing density, a series of SiC powder mixtures were systematically prepared using five distinct particle size fractions: 37 µm, 23 µm, 12 µm, 4 µm, and 0.6 µm. Blending was performed by starting with a coarse base powder and incrementally adding finer powders in proportions related to the estimated interparticle void volume of the larger particles. Apparent and tapped densities were measured for each blend to assess how the addition of medium and fine powders affected packing behavior. Figure 6 presents the evolution of powder composition and corresponding packing densities across a full set of unimodal, bimodal, and trimodal mixtures.

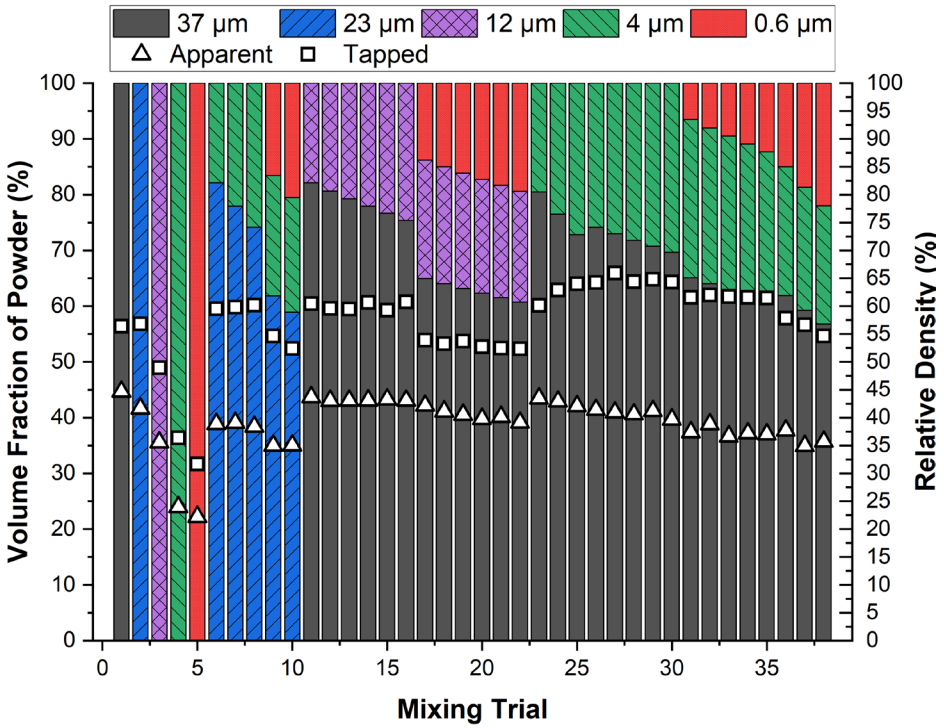

Figure 6: Volume fraction composition and corresponding packing densities (apparent and tapped) for a series of SiC powder blends. Each stacked bar represents a unique powder mixture composed of varying ratios of five particle size fractions: 37 µm, 23 µm, 12 µm, 4 µm, and 0.6 µm. These measurements are associated with the y-axis on the left side of the figure. Apparent density (open squares) and tapped density (open triangles) were measured for each blend to evaluate packing performance. These measurements are associated with y-axis on the right side of the figure.

The packing density data reveal clear trends associated with the progression from unimodal to bimodal and trimodal powder blends. As shown in Figure 6, the base powders (37 µm and 23 µm) exhibit relatively high packing density on their own, with tapped densities exceeding 55%. The introduction of medium-sized powders (e.g., 12 µm and 4 µm) into these base powders generally improved packing density up to a point. Notably, the largest gains in both apparent and tapped density were observed when the added powder volume was approximately 50% of the calculated void volume of the base powder. This supports the theoretical expectation that partial void filling with a complementary size fraction enhances packing efficiency.

As more medium powder was added beyond this point, the rate of density improvement began to plateau, indicating diminishing returns. In several cases, excessive addition of smaller particles led to a reduction in apparent density—likely due to increased interparticle friction, agglomeration, or disruption of flow characteristics. For blends that included a third (finer) powder such as 0.6 µm particles, a similar trend was observed: moderate additions contributed to slight gains or stabilization in tapped density, while excessive fine content led to reductions, particularly in apparent density. These outcomes highlight the importance of balancing void filling with powder flowability and suggest that there is an optimal window for multi-modal blending in SiC systems.

3.2 ACTUAL VERSUS PREDICTED PACKING DENSITY

Figure 7 shows the predicted versus experimentally measured packing densities for bimodal blends of 37 µm and 4 µm SiC powders. The theoretical curve (black squares) was generated using a particle packing model that estimates total packing density as a function of the volume fraction of the larger powder in the blend. This model assumes ideal spherical particles and no agglomeration, providing a best-case scenario for packing efficiency.

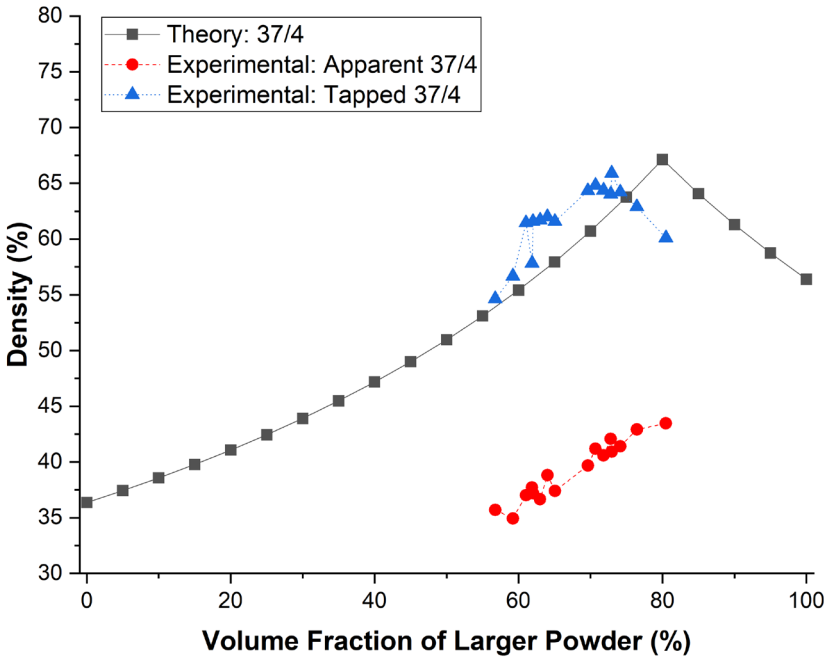

Figure 7: Theoretical packing for increasing volume fraction of two powders in a bimodal blend (4 and 37 microns). Experimental values for apparent and tapped densities of these powder blends suggest that the theoretical values align closely with tapped densities, at least for bimodal blends.

Experimental values for both apparent and tapped density are plotted for comparison. Apparent densities (red circles) were consistently lower than both theoretical and tapped values, reflecting the looser arrangement of particles in the absence of compaction. Tapped densities (blue triangles), obtained after mechanical tapping, more closely approached the theoretical predictions and followed a similar trend—rising with increasing large particle fraction and reaching a maximum near 75–80% before declining. This agreement suggests that the voids created by the coarse 37 µm particles are effectively filled by the 4 µm particles up to an optimal blend ratio, beyond which excess fines may disrupt packing efficiency.
The deviation between theory and experiment—especially for apparent density—can be attributed to factors not captured in the model, such as particle irregularity, surface roughness, and interparticle friction. Nonetheless, the comparison validates the general trend predicted by the model and highlights the importance of optimizing blend ratios to maximize packing density in real-world systems.

3.3 RECYLABILITY

To assess the stability and reusability of the bimodal powder blend (37 µm / 4 µm) in the BJAM process, particle size distribution (PSD) was measured at various stages of the printing workflow over eight consecutive print cycles. The goal was to determine whether mechanical handling, transport, or printing operations caused segregation or preferential depletion of specific particle size fractions. Samples were collected from five key locations in the system: the hopper before printing, the job box after printing, the overflow reservoir, the hopper after printing, and after sieving of the reclaimed powder. These measurements shown in Figure 8, Figure 9, Figure 10, Figure 11, Figure 12, Figure 13, Figure 14, and Figure 15 provide insight into how well the multimodal blend retains its integrity during repeated use in binder jetting.

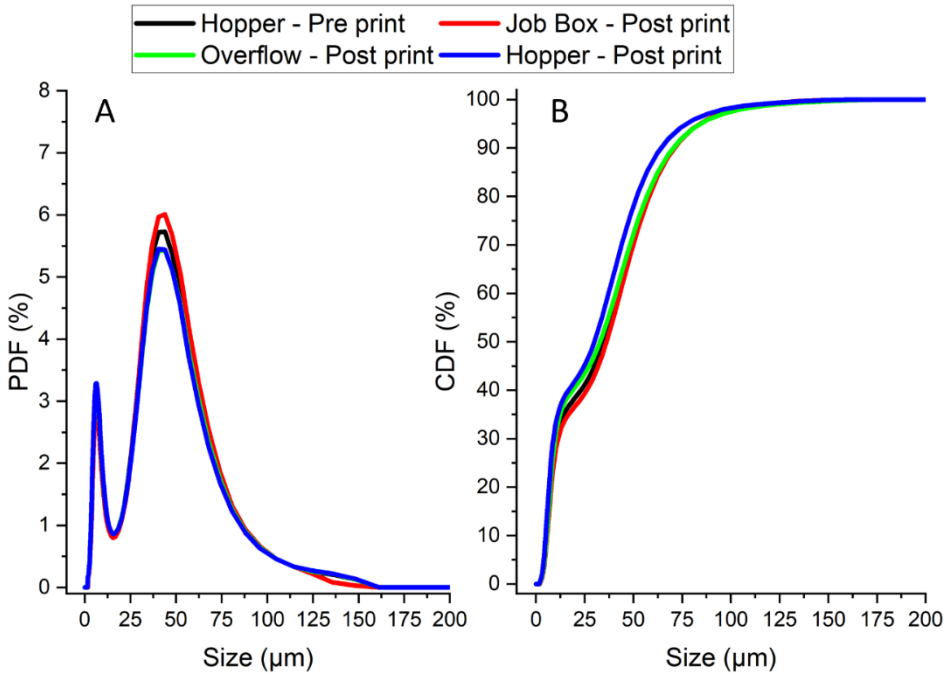

Figure 8: A) PDF and B) CDF of the bimodal powder after the first printing cycle.

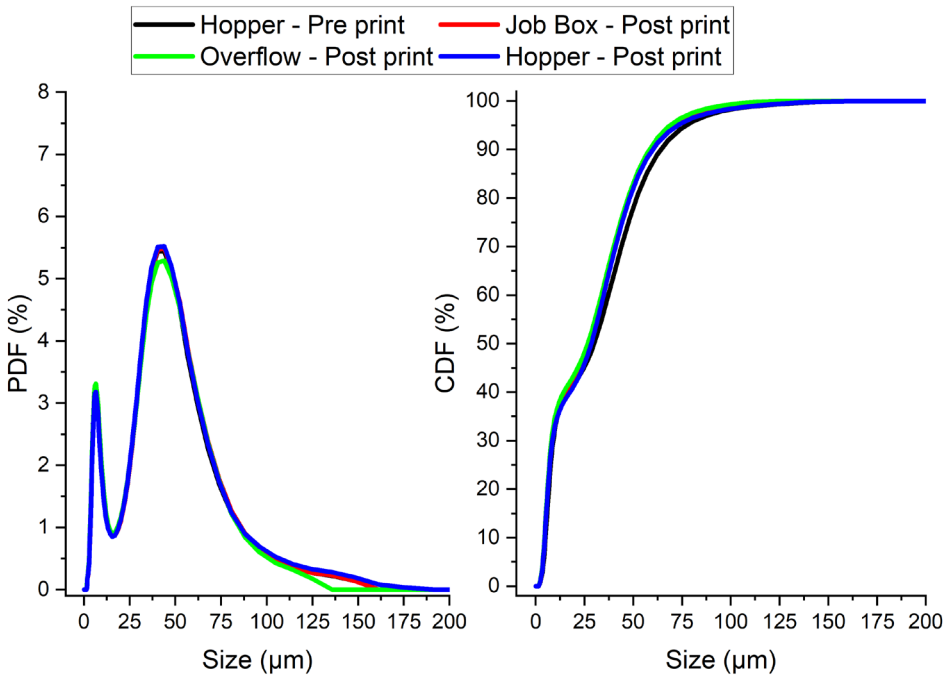

Figure 9: A) PDF and B) CDF of the bimodal powder after the second printing cycle.

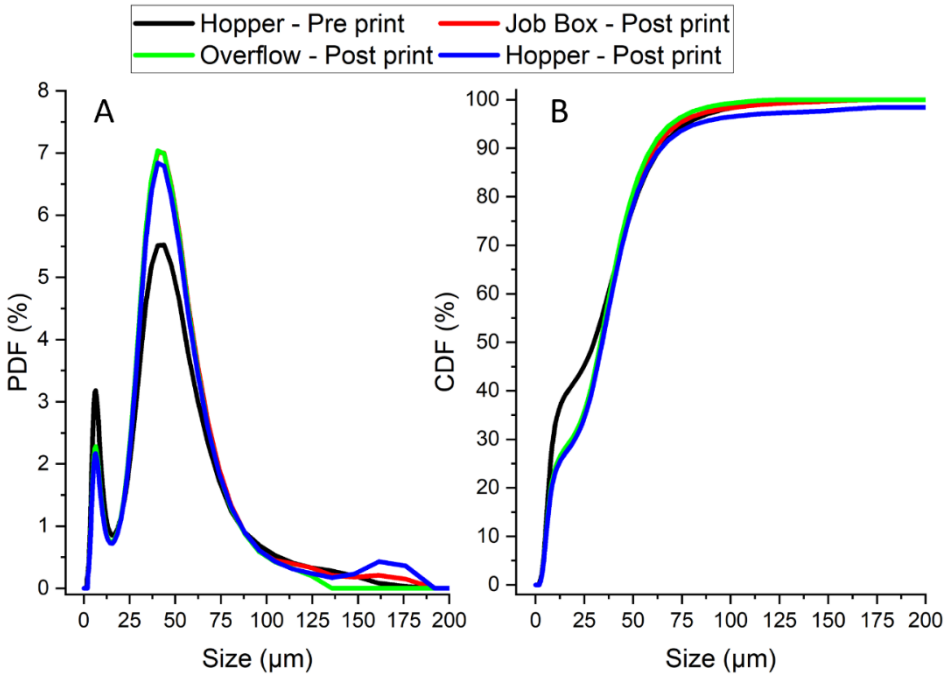

Figure 10: A) PDF and B) CDF of the bimodal powder after the third printing cycle.

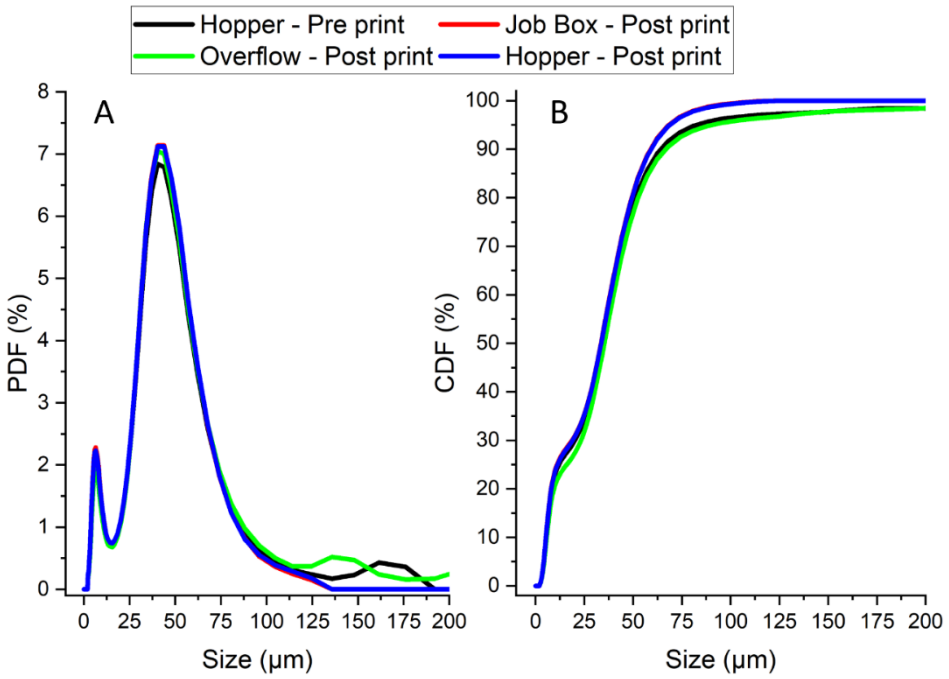

Figure 11: A) PDF and B) CDF of the bimodal powder after the fourth printing cycle.

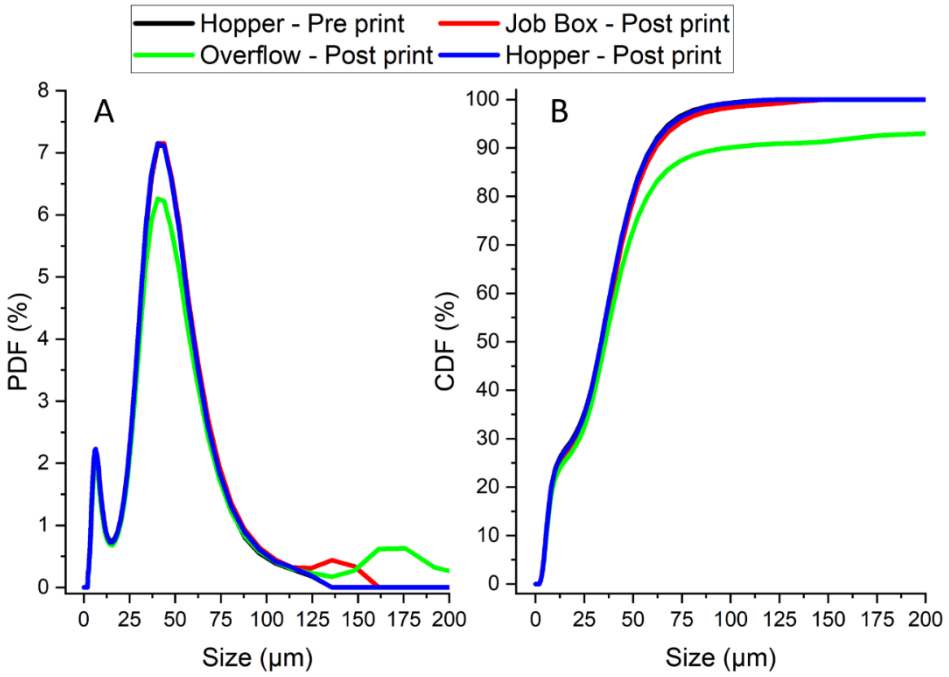

Figure 12: A) PDF and B) CDF of the bimodal powder after the fifth printing cycle.

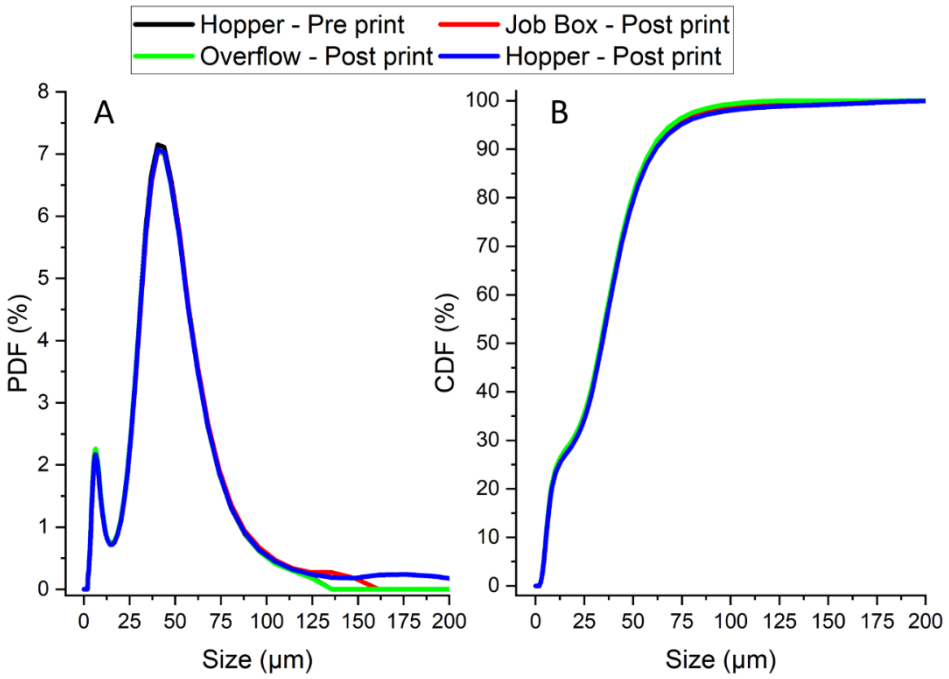

Figure 13: A) PDF and B) CDF of the bimodal powder after the sixth printing cycle.

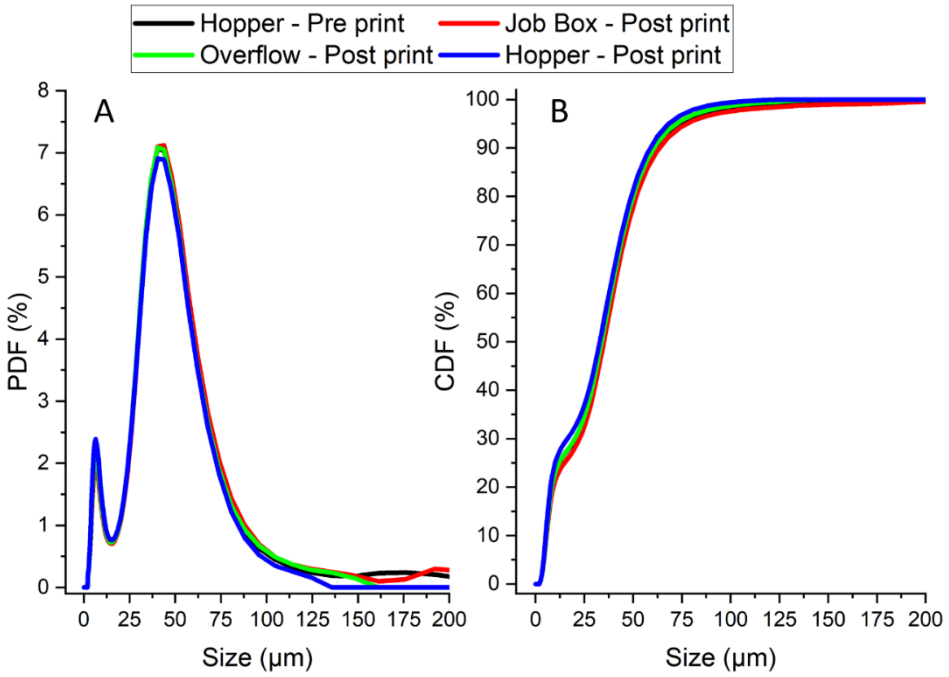

Figure 14: A) PDF and B) CDF of the bimodal powder after the seventh printing cycle.

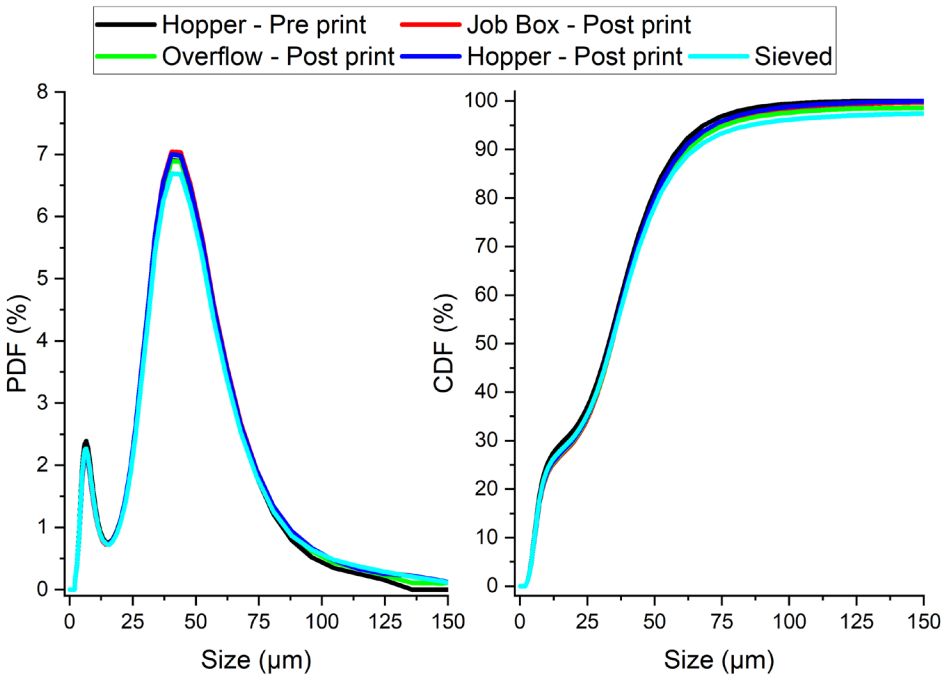

Figure 15: A) PDF and B) CDF of the bimodal powder after the eighth printing cycle.

As shown in Figure 15, the PDFs and CDFs from all five sampling points overlap closely, with no discernible shifts in peak particle size or distribution shape. This strong agreement across all curves indicates that no significant particle segregation or size-based fractionation occurred over the course of eight print runs. The consistency of the PSD suggests that the bimodal blend remains stable throughout the powder handling system, including mechanical spreading, overflow capture, and post-print recycling. These findings support the feasibility of reusing multimodal SiC powders in BJAM without significant degradation of their packing characteristics or particle size uniformity.

3.4 FINAL STRENGTH

The powder blend with the highest predicted packing density—an 73% volume fraction in the 37/4 µm bimodal system—was selected for binder jet printing and subsequent densification via chemical vapor infiltration (CVI). Green parts were printed using this blend, and green density was calculated from caliper-based volume and mass measurements. The resulting green densities ranged from 44.44% to 48.45%, indicating effective powder packing prior to infiltration.

Following densification, specimens were subjected to flexural strength testing to evaluate mechanical performance. A total of 10 samples were produced and tested for each powder blend. Table 2 presents the average flexural strength, standard deviation, and Weibull scale and shape parameters for specimens made from both unimodal and bimodal powder distributions.

Table 1: Descriptive statistical values

Powder	Average Strength MPa	P value	Standard deviation MPa	Scale parameter MPa	Shape parameter
Unimodal	208.42	<0.001	16.87	215.37	17.66
Bimodal	220.39		13.56	226.66	17.64

Results show a statistically significant improvement in flexural strength for parts printed with the bimodal blend compared to the unimodal counterpart ($p < 0.001$). The bimodal specimens achieved a higher mean strength and lower standard deviation, suggesting more consistent mechanical performance. Additionally, Weibull analysis indicated that the bimodal specimens had slightly higher scale parameters and comparable shape parameters (both >17), reflecting improved strength and reliability.
It is important to note, however, that the minimum number of samples required for a formal Weibull analysis was not achieved. As such, the Weibull statistics are presented for qualitative comparison only and should not be interpreted as meeting full statistical rigor per ASTM standards.

4. DISCUSION

4.1 PACKING EFFICIENCY OF BIMODAL AND TRIMODAL BLENDS

This study explored the packing behavior of bimodal and trimodal SiC powder blends, aiming to maximize green density for binder jet additive manufacturing (BJAM). According to packing theory, adding smaller particles to a powder system can fill the interparticle voids between larger particles, leading to increased bulk density. This trend was confirmed in the bimodal blends studied here, where the combination of 37 μm and 4 μm powders yielded the highest packing efficiency.
However, when a third, finer powder (0.6 μm) was introduced to create trimodal blends, a consistent reduction in density was observed. This was attributed to particle agglomeration, increased interparticle friction, and wall effects. The bimodal interaction between the 4 μm and 0.6 μm powders (~6.7:1 size ratio) falls just below the commonly accepted range of 7–10:1 for optimal packing [14], while the 37 μm and 0.6 μm powders have a much larger size ratio (~62:1). Although theoretical models predicted slightly higher packing at high volume fractions of coarse powder (≥80%) for the 37/0.6 μm combination, the practical challenges of handling ultrafine powders outweighed potential gains.
Ultimately, the 37/4 μm bimodal blend was selected for further study and printing due to its superior packing behavior and ease of handling.

4.2 LIMITATIONS AND GENERALIZATION OF FINDINGS

While the experimental results confirm theoretical expectations for bimodal systems, there are limitations to this study. Only one material (SiC) and three particle sizes were used, which constrains generalization to other materials or size distributions. Additionally, the use of a powder splitter for sample collection is reliable for same-material blends but may not provide accurate mixing for systems with different materials or densities. Nonetheless, the methodology developed—particularly the use of theoretical void filling to guide blend design—can be applied to a wide range of powder systems. The use of a V-blender for bulk powder preparation further enhances reproducibility and homogeneity across diverse materials [28,29].

4.3 RATIONALE FOR USING TAPPED DENSITY

Tapped density was chosen as the benchmark for evaluating maximum achievable packing in loose powder beds. It represents the densest condition obtainable without applying external compression and is commonly used in powder metallurgy and additive manufacturing. Since actual BJAM powder bed densities fall between the apparent and tapped values [36–38], tapped density provides a practical upper bound for evaluating blend performance. The goal in blending was to approach this tapped limit as closely as possible with flowable, printable powder blends.

4.4 COMPARISON WITH LITERATURE

Our findings are in strong agreement with prior analytical and experimental studies. Du et al. [17] reported that bimodal blends of irregularly shaped SiC particles achieved maximum packing at 75.9% volume fraction of coarse powder, with a peak tapped density of 70.61% theoretical. Feng et al. [30] also observed peak packing at 75% coarse fraction, achieving 70.1% tapped density. The current study focused on targeting specific void fill fractions and achieved maximum packing at an estimated 85% void fill (~42% coarse powder by volume). Although absolute densities were somewhat lower than reported in the literature, this discrepancy is likely due to differences in particle morphology and agglomeration behavior. Figure 6 further illustrates how the theoretical maximum packing density of each bimodal pair varies with blend ratio. While the 37/0.6 μm blend may outperform 37/4 μm at very high coarse powder fractions, the fine powder's agglomeration and poor flow characteristics limit its practical utility.

4.5 POWDER RECYCLABILITY AND PSD STABILITY

A notable contribution of this work is the evaluation of powder recyclability using particle size distribution (PSD) measurements across eight print cycles. While prior studies have reported PSD data for bimodal powders prior to printing [15–17,30–36], few have investigated how the PSD changes throughout the BJAM process.

In this study, PSD was measured at multiple stages—before printing (hopper), after printing (job box, hopper, overflow), and after sieving. The resulting PDFs and CDFs (Figure 15 and Supplementary S1) showed substantial overlap across all sampling locations, indicating that no significant segregation or particle size drift occurred. This finding supports the homogeneity and recyclability of the 37/4 μm bimodal blend over multiple print runs.

4.6 MECHANICAL PERFORMANCE OF PRINTER PARTS

Mechanical testing confirmed that the improved powder packing translated into better part performance. Specimens printed from the bimodal blend exhibited significantly higher flexural strength than those printed from the unimodal powder ($p < 0.001$), along with lower variability. This aligns with prior studies showing that enhanced packing and reduced porosity improve mechanical strength in BJAM of SiC [30] and other materials, including Inconel 718 processed via laser powder bed fusion [31].

Although Weibull shape and scale parameters were calculated for comparative purposes, the sample count was below the minimum required for a statistically rigorous Weibull analysis. These results are therefore offered as a qualitative comparison of strength consistency between the unimodal and bimodal specimens.

5. CONCLUSIONS

This study demonstrated that bimodal powder blends of silicon carbide significantly improve powder packing density in binder jet additive manufacturing (BJAM) compared to unimodal blends. Although some trimodal blends exhibited local increases in packing, the overall effect was a reduction in density relative to optimized bimodal systems. These results highlight the importance of selecting appropriate size ratios and volume fractions in multimodal blending, and the potential drawbacks of adding excessively fine particles.

Parts printed from the optimal bimodal blend (37/4 μm) not only exhibited higher green density but also achieved significantly greater flexural strength after densification. This mechanical improvement further supports the use of bimodal powders to enhance part performance in BJAM.

A major outcome of this work is the finding that no measurable powder separation or segregation occurred during eight consecutive print cycles, including powder handling, overflow recovery, and sieving. The stability of the particle size distribution (PSD) across multiple recycling stages suggests that bimodal blends of the same material can maintain homogeneity and consistent performance over repeated use—a critical factor for sustainable powder reuse in additive manufacturing.

While this study focused on a specific SiC powder system, the blending approach and findings provide a framework for designing and validating multimodal powder systems in other material contexts. These insights have broad implications for improving green density, mechanical properties, and powder recyclability in powder bed AM processes, supporting more efficient and reliable additive manufacturing workflows.

6. ACKNOWLEDGEMENT

The project was funded by Advanced Research Projects Agency–Energy (ARPA-e) under OPEN 2021 program. The project would like to acknowledge the support from Dimensional Energy Inc. particularly Dr. Bradley J. Brennan and Dr. Bhargavi Mummareddy for specifying the design and process requirements.

APPENDIX A. WORKS CITED

APPENDIX A. WORKS CITED

[1] S. Yerazunis, S.W. Cornell, B. Wintner, Dense Random Packing of Binary Mixtures of Spheres, Nature. 207 (1965) 835–837. https://doi.org/10.1038/207835a0.

[2] W.M. Visscher, M. Bolsterli, Random packing of equal and unequal spheres in two and three dimensions, Nature. 239 (1972) 504–507. https://doi.org/10.1038/239504a0.

[3] M.J. Powell, Computer-simulated random packing of spheres, Powder Technol. 25 (1980) 45–52. https://doi.org/10.1016/0032-5910(80)87007-0.

[4] G.T. Nolan, P.E. Kavanagh, Computer simulation of random packing of hard spheres, Powder Technol. 72 (1992) 149–155. https://doi.org/10.1016/0032-5910(92)88021-9.

[5] R. Jullien, P. Meakin, Simple Three-Dimensional Models for Ballistic Deposition with Restructuring, Europhys. Lett. 4 (1987) 1385–1390. https://doi.org/10.1209/0295-5075/4/12/008.

[6] J.E. Ayer, F.E. Soppet, Vibratory Compaction: I, Compaction of Spherical Shapes, J. Am. Ceram. Soc. 48 (1965) 180–183. https://doi.org/10.1111/j.1151-2916.1965.tb14708.x.

[7] J.E. Ayer, F.E. Soppet, Vibratory Compaction: II, Compaction of Angular Shapes, J. Am. Ceram. Soc. 49 (1966) 207–210. https://doi.org/10.1111/j.1151-2916.1966.tb13235.x.

[8] W. Soppe, Computer simulation of random packings of hard spheres, Powder Technol. 62 (1990) 189–197. https://doi.org/10.1016/0032-5910(90)80083-B.

[9] T.M. Abu-Lebdeh, R. Damptey, L.M. Ungureanu, F.I.T. Petrescu, A Ternary Model for Particle Packing Optimization, J. Compos. Sci. 6 (2022) 113. https://doi.org/10.3390/jcs6040113.

[10] J. Zheng, W.B. Carlson, J.S. Reed, The packing density of binary powder mixtures, J. Eur. Ceram. Soc. 15 (1995) 479–483. https://doi.org/10.1016/0955-2219(95)00001-B.

[11] A.K.H. Kwan, K.W. Chan, V. Wong, A 3-parameter particle packing model incorporating the wedging effect, Powder Technol. 237 (2013) 172–179. https://doi.org/10.1016/j.powtec.2013.01.043.

[12] X. Ye, Y. Li, Y. Ai, Y. Nie, Novel powder packing theory with bimodal particle size distribution-application in superalloy, Adv. Powder Technol. 29 (2018) 2280–2287. https://doi.org/10.1016/j.apt.2018.06.012.

[13] R.F. Fedors, R.F. Landel, An Empirical method of estimating the void fraction in mixtures of uniform particles of different size, Powder Technol. 23 (1979) 225–231. https://doi.org/10.1016/0032-5910(79)87011-4.

[14] A.B. Yu, R.P. Zou, N. Standish, Modifying the linear packing model for predicting the porosity of nonspherical particle mixtures, Ind. Eng. Chem. Res. 35 (1996) 3730–3741. https://doi.org/10.1021/ie950616a.

[15] Y. Bai, G. Wagner, C.B. Williams, Effect of Particle Size Distribution on Powder Packing and Sintering in Binder Jetting Additive Manufacturing of Metals, J. Manuf. Sci. Eng. 139 (2017) 1–6. https://doi.org/10.1115/1.4036640.

[16] H. Miyanaji, K.M. Rahman, M. Da, C.B. Williams, Effect of fine powder particles on quality of binder jetting parts, Addit. Manuf. 36 (2020) 101587. https://doi.org/10.1016/j.addma.2020.101587.

[17] W. Du, M. Singh, D. Singh, Binder jetting additive manufacturing of silicon carbide ceramics: Development of bimodal powder feedstocks by modeling and experimental methods, Ceram. Int. 46 (2020) 19701–19707. https://doi.org/10.1016/j.ceramint.2020.04.098.

[18] C.L. Cramer, H. Armstrong, A. Flores-Betancourt, L. Han, A.M. Elliott, E. Lara-Curzio, T. Saito, K. Nawaz, Processing and properties of SiC composites made via binder jet 3D printing and infiltration and pyrolysis of preceramic polymer, Int. J. Ceram. Eng. Sci. 2 (2020) 320–331. https://doi.org/10.1002/ces2.10070.

[19] T. Koyanagi, K. Terrani, S. Harrison, J. Liu, Y. Katoh, Additive manufacturing of silicon carbide for nuclear applications, J. Nucl. Mater. 543 (2021) 152577. https://doi.org/10.1016/j.jnucmat.2020.152577.

[20] T.G. Lach, A.G. Le Coq, K.D. Linton, K.A. Terrani, T.S. Byun, Characterization of radiation damage in 3D printed SiC, J. Nucl. Mater. 559 (2022) 153459. https://doi.org/10.1016/j.jnucmat.2021.153459.

[21] G. Vasudevamurthy, M. Trammell, D. Richardson, B. Jolly, A. Nelson, G. Helmreich, A. Schumacher, T. Smuin, K. Terrani, Fabrication and characterization methodology of transformational challenge reactor fuel form, Trans. Am. Nucl. Soc. 122 (2020) 357–359. https://doi.org/10.13182/T122-32474.

[22] K.A. Terrani, T. Lach, H. Wang, A. Le Coq, K. Linton, C. Petrie, T. Koyanagi, T.S. Byun, Irradiation stability and thermomechanical properties of 3D-printed SiC, J. Nucl. Mater. 551 (2021) 152980. https://doi.org/10.1016/j.jnucmat.2021.152980.

[23] T. Byun, T. Lach, C. Parish, H. Wang, A. Trofimov, D. Collins, A. Le Coq, K. Linton, M. Richardson, B. Jolly, M. Trammell, A. Schumacher, G. Vasudevamurthy, T. Koyanagi, K. Terrani, Mechanical and Thermophysical Properties of 3D-Printed SiC before and after Neutron Irradiation – FY21, Oak Ridge, TN (United States), 2021. https://doi.org/10.2172/1814305.

[24] T. Byun, B. Garrison, H. Wang, A. Trofimov, T. Lach, C. Parish, M. Richardson, B. Jolly, M. Trammell, A. Schumacher, G. Vasudevamurthy, T. Koyanagi, K. Terrani, Mechanical and Thermophysical Properties of 3D-Printed SiC-FY20, Oak Ridge, TN (United States), 2020. https://doi.org/10.2172/1632077.

[25] American Society for Testing and Materials, Test Methods for Flow Rate of Metal Powders Using the Hall Flowmeter Funnel, Annu. B. ASTM Stand. i (2020) 213–216. https://doi.org/10.1520/B0213-20.

[26] American Society for Testing and Materials, Standard Test Method for Tap Density of Metal Powders and Compounds, B527. i (2015) 15–18. https://doi.org/10.1520/B0527-24.2.

[27] American Society for Testing and Materials, Standard Test Method for Flexural Strength of Advanced Ceramics at Ambient Temperature, Order A J. Theory Ordered Sets Its Appl. 94 (1996) 1–15. https://doi.org/10.1520/C1161-18.1.

[28] Q. Shi, S. Yang, Y. Sun, B. Van Meerbeek, C. Politis, In-situ modulating laminated microstructure of α+β+TiC in titanium composites by laser powder bed fusion of Mo2C/Ti powder mixture towards biomedical applications, Mater. Sci. Eng. A. 857 (2022) 144101. https://doi.org/10.1016/j.msea.2022.144101.

[29] S. Feng, S. Guan, S. Zhang, S. Mooraj, M. Luebbe, X. Fan, K.A. Beyer, T. Li, J. Liu, J. Kong, P.K. Liaw, H. Wen, S. Gerasimidis, W. Chen, Ultrafine-grained Fe-TiB2 high-modulus nanocomposite steel with high strength and isotropic mechanical properties by laser powder bed fusion, Addit. Manuf. 70 (2023) 103569. https://doi.org/10.1016/j.addma.2023.103569.

[30] K. Feng, S. Hu, W. Zhao, J. Sun, Y. Mao, D. Cai, J. Wu, Q. Wei, Bimodal powder optimization in SiC binder jetting for mechanical performance, Int. J. Mech. Sci. 274 (2024) 109278. https://doi.org/10.1016/j.ijmecsci.2024.109278.

[31] S.A. Farzadfar, M.J. Murtagh, N. Venugopal, Impact of IN718 bimodal powder size distribution on the performance and productivity of laser powder bed fusion additive manufacturing process, Powder Technol. 375 (2020) 60–80. https://doi.org/10.1016/j.powtec.2020.07.092.

[32] Q. Li, B. Zhang, Y. Wen, G. Chen, Y. Wang, P. Wang, X. Qu, A comprehensive study of tantalum powder preparation for additive manufacturing, Appl. Surf. Sci. 593 (2022) 153357. https://doi.org/10.1016/j.apsusc.2022.153357.

[33] Y. Ekubaru, O. Gokcekaya, T. Ishimoto, K. Sato, K. Manabe, P. Wang, T. Nakano, Excellent strength–ductility balance of Sc-Zr-modified Al–Mg alloy by tuning bimodal microstructure via hatch spacing in laser powder bed fusion, Mater. Des. 221 (2022) 110976. https://doi.org/10.1016/j.matdes.2022.110976.

[34] X. Xi, D. Lin, X. Song, X. Luo, R. Ma, Z. Shi, H. Bian, W. Fu, Z. Dong, C. Tan, Strength-plasticity transition mechanism after the solution treatment of GH3230 superalloy fabricated via laser powder bed fusion, Mater. Sci. Eng. A. 876 (2023) 145124. https://doi.org/10.1016/j.msea.2023.145124.

[35] M. Opprecht, J.P. Garandet, G. Roux, C. Flament, M. Soulier, A solution to the hot cracking problem for aluminium alloys manufactured by laser beam melting, Acta Mater. 197 (2020) 40–53. https://doi.org/10.1016/j.actamat.2020.07.015.

[36] S.K. Gupta, N. Shahidsha, S. Bahl, D. Kedaria, S. Singamneni, P.K.D.V. Yarlagadda, S. Suwas, K. Chatterjee, Enhanced biomechanical performance of additively manufactured Ti-6Al-4V bone plates, J. Mech. Behav. Biomed. Mater. 119 (2021) 104552. https://doi.org/10.1016/j.jmbbm.2021.104552.